Intrusion Characteristics in the Antarctic Polar Front[1]

JOHN M. TOOLE

Pacific Marine Environmental Laboratory, NOAA, Seattle, WA 98105

(Manuscript received 1 December 1980, in final form 9 March 1981)

ABSTRACT

Data obtained on two cruises to the Antarctic Polar Front are used to investigate the nature of thermohaline intrusions in the front. These data, obtained in the Drake Passage and south of New Zealand, include CTD time series made relative to neutrally buoyant vertical-current meters, temperature data from these floats, and small-scale CTD sections. Analysis of these data is divided into a study of temporal persistance and an examination of the spatial structure of the intrusions. The study of intrusion time scales is hampered by the presence of large spatial gradients in the intrusion field. This study suggests that features are persistent for several days but additional measurements appear necessary to resolve the intrusion decay process. The length scales of intrusions are found to vary within the frontal zone. Near the region of maximum lateral gradients in the front, length scales of 5 to 10 km are observed, while elsewhere scales of only 1 km are found. It is suggested that these small, isolated leaves of fluid are old intrusions that have been sheared and advected from their generation site. Several pieces of circumstantial evidence are presented to support the hypothesis that intrusions are driven by salt fingering, and good agreement between the observations and the results of a dynamical model of intrusions driven by salt fingers is noted. Finally, application of a statistical model for intrusive variance predicts that intrusions may effect constant lateral eddy diffusivities in fronts provided the small-scale vertical diffusivity is constant.

1. Introduction

a. Overview

The nature of intrusive finestructure associated with oceanic fronts has been studied extensively in recent years. Three papers have dealt exclusively with the intrusions found in the Antarctic Polar Front. Gordon *et al.* (1977, hereafter GGT) presented a series of STD profiles from the frontal zone in the western Scotia Sea. Georgi (1978) discussed several XBT experiments designed to sample the intrusion length scales, along with STD and XBT observations to determine the time scales of the intrusions. Joyce *et al.* (1978, hereafter JZT) discussed CTD and profiling-current-meter measurements taken in the Drake Passage.

On the basis of these and other studies, several theories were developed which deal with the dynamics of intrusions and their effects on larger-scale fields. Specifically, intrusions are believed to be driven by salt fingers (e.g., Stern, 1967; Turner, 1978), and to effect lateral mixing across the front (e.g., Joyce, 1977). The intrusion theories evolved from studies of the structure of the intrusions and their evolution with time. As these observations are strongly convolved in space and time though, they are subject to various interpretations.

This paper discusses the results of several experiments designed to separate observations of the spatial structure of the intrusions from those of their temporal evolution. These experiments were performed on two cruises to the APF. The first cruise took place in March 1976 aboard the R.V. *Thompson* in the Drake Passage (Joyce, 1976). Some of the results from that cruise have been discussed by Joyce and Patterson (1977) and JZT. The second cruise, aboard the R.V. *Knorr* south of New Zealand, took place in November of 1978 (Bryden and Joyce, 1979). The data from the cruises discussed here include temperature and salinity time series from CTD stations made relative to neutrally buoyant floats, temperature data from these floats, and small-scale CTD sections.

Much of the following analysis is based on the previous studies of GGT, JZT and Georgi (1978). A review of their results is presented below before discussing the new observations. It will be shown that the nature of the finestructure appears strongly dependent on the characteristics of the frontal scale fields. Therefore, Section 2 is devoted to a brief description of the frontal properties at the times when finestructure measurements were made. The

[1] Woods Hole Oceanographic Institution Contribution No. 4725. NOAA/ERL Pacific Marine Environmental Laboratory Contribution No. 499.

0022-3670/81/060780-14$07.50

temporal behavior of the intrusions is discussed in Section 3, while Section 4 investigates their spatial structure. Finally, Section 5 discusses the thermohaline characteristics of the features and presents evidence for double-diffusive mixing.

b. Previous observations

The thermohaline finestructure in the Antarctic Polar Front is characterized by numerous inversions in vertical temperature and salinity profiles, probably the product of lateral advection across the frontal zone (GGT). These features dominate the thermohaline variability on vertical scales smaller than 100 m at depths from 100 to roughly 1000 m in the frontal zone (GGT, JZT). The vertical spectra of temperature and salinity anomalies are red (JZT) with a vertical wavenumber slope between -2 and -3. Vertical-gradient spectra exhibit enhanced energy density at wavelengths between 100 and 30 m.

Horizontal length scales for the intrusive finestructure were first estimated by GGT from a series of STD casts made from a drifting ship. The range of alongfront length scales quoted was 0.3–0.7 km for an aspect ratio (intrusion height divided by length) of 0.1. Georgi (1978) estimated both along- and crossfront length scales from a set of closely spaced XBT's. He found an anisotropy in the intrusion field with longer scales in the along-front direction. Along- and crossfront aspect ratios found in this study for features with vertical wavelengths of order 100 m were 0.03 and 0.10, respectively. Along-front intrusion length scales also were estimated by JZT with data from a 28 h CTD time series. An along-front aspect ratio computed with these data was order 0.01.

Measurements of the time scale of the intrusive variability are generally complicated by spatial gradients also present in the intrusion field. Individual intrusions were observed for 5 h by GGT during their ship drift while JZT computed a coherence time scale of 5 h with their data. These results were interpreted as spatial variability as described above, not intrusion variations with time. Georgi (1978) computed the loss of coherence of the finestructure with time using STD and XBT time-series data. His results displayed a rapid fall-off of coherence with time and vertical wavenumber. The coherence between features with vertical wavelengths of 100 to 250 m was significantly different from zero for periods longer than 1 h. At smaller wavelengths, 50 to 100 m, this period fell to just over 15 min. Phase randomization by internal-wave vertical advections and spatial gradients in the intrusion field could have acted to reduce the coherence calculated by Georgi.

The thermohaline characteristics of the intrusions were also investigated in these studies. Since the temperature and salinity anomalies are correlated in the finestructure, there is little density signal associated with the features. A regression between temperature and salinity anomalies by GGT yielded a value for the nondimensionalized ratio of the anomalies which was indistinguishable from 1.0. This led GGT to use the term "density compensating" to describe the temperature and salinity anomalies of the finestructure. The density-compensating nature of the finestructure was investigated by JZT. A plot of the non-dimensionalized ratio of the vertical-temperature-gradient spectra to that for salinity versus vertical wavenumber showed that on scales >20 m the finestructure appeared density-compensating (the above ratio equal to 1.0). On smaller scales, this ratio fell below 1.0 on account of an excess of salinity-gradient variance. In physical space a calculation of vertical stability found marginally weaker stratification at depths where the vertical temperature and salinity gradients were positive as compared to depths where the vertical gradients were negative. These results suggested the finestructure was not density-compensating on small vertical scales, but this result may be an instrumental artifact (Millard, *et al.*, 1980; Horne and Toole, 1980).

The intrusions observed in the CTD time series discussed by JZT appeared on slightly different potential density surfaces. This was interpreted by JZT as the advection of sloping features past the observation site. The slope of the intrusions relative to the density surfaces in the across-front direction was estimated to be between 0.02 and 0.04, with features deepening towards warmer water. The sense of this slope (warm intrusions rising and cold ones sinking) is consistent with the hypothesis that the intrusions are driven by vertical salt-finger fluxes (Turner, 1978).

2. Frontal scale fields

The Antarctic Polar Front is a circumpolar water-mass boundary separating the cold, fresh surface waters of the Southern Ocean with its characteristic temperature-minimum layer from the warmer, more saline subantarctic waters (see Gordon, 1971). The large scale characteristics of this front in the Drake Passage and South of New Zealand are presented in this section.

The hydrographic structure of the polar front in the Drake Passage for the time period of the *Thompson* cruise is presented by JZT. The time evolution of the front has also been documented by Joyce and Patterson (1977). During the cruise, the front evolved rapidly and formed a cold-core ring which was mapped by a two-ship operation (Joyce, 1976; Patterson and Sievers, 1976). Finestructure observations obtained in the frontal zone before the

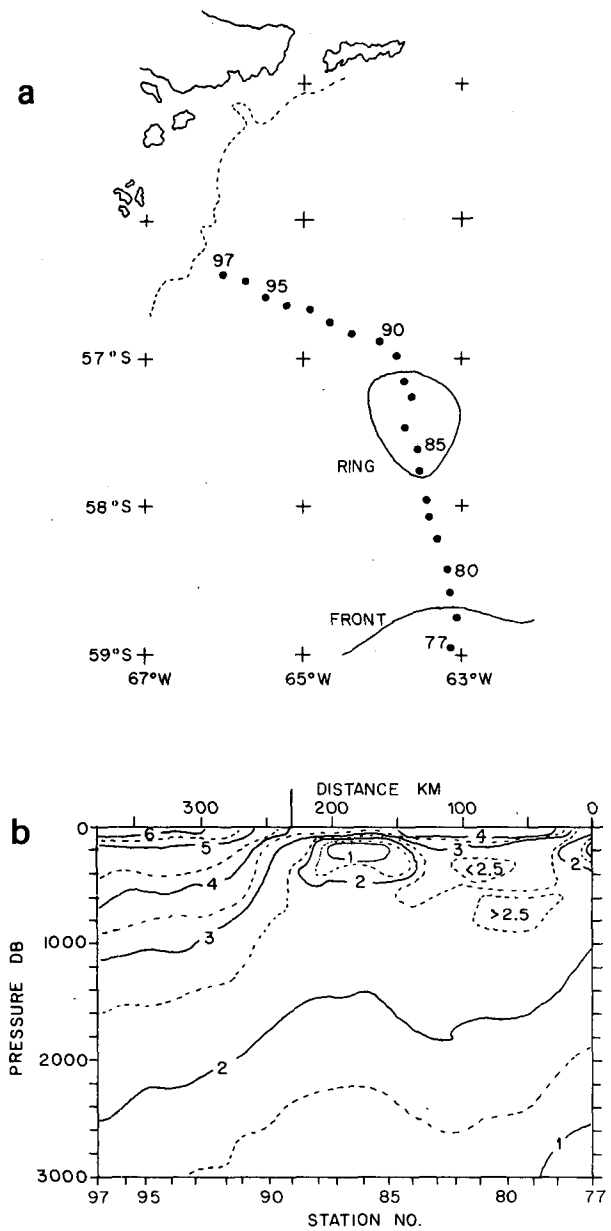

FIG. 1. The station position map (a), and temperature section (b), from a large-scale CTD section which spanned the region of the CTD time series. The positions of the Antarctic Polar Front and the cold-core ring at the time of the section are shown in (a). The time series was taken near CTD 80, just south of the cold pool of water centered at 200 db about CTD 81 in (b).

ring formed are discussed by JZT. Measurements taken in the re-established front, several days after the ring separated, are presented here.

A large-scale CTD section spanned the observational site in the re-established front (Fig. 1). Neutrally buoyant vertical-current meters (VCM's) were deployed in the front at 400 and 600 m depth, and shipboard measurements were made relative to the floats. Temperature data obtained around the floats were consistent with the thermal field near CTD 80 in Fig. 1b. The local horizontal temperature gradient in the region was a factor of 4 weaker than that observed by JZT before the ring event, and, at depths below 200 m, had the opposite sign because of a cold pool of water located just north of the site (see Fig. 1b). The maximum frontal gradients were located south of the observational site, near the termination of the temperature-minimum layer seen between stations 77 and 78 in Fig. 1b. The section suggests that finestructure measurements made near station 80 may be in a far-field regime for the interleaving, away from the large horizontal gradients of the front.

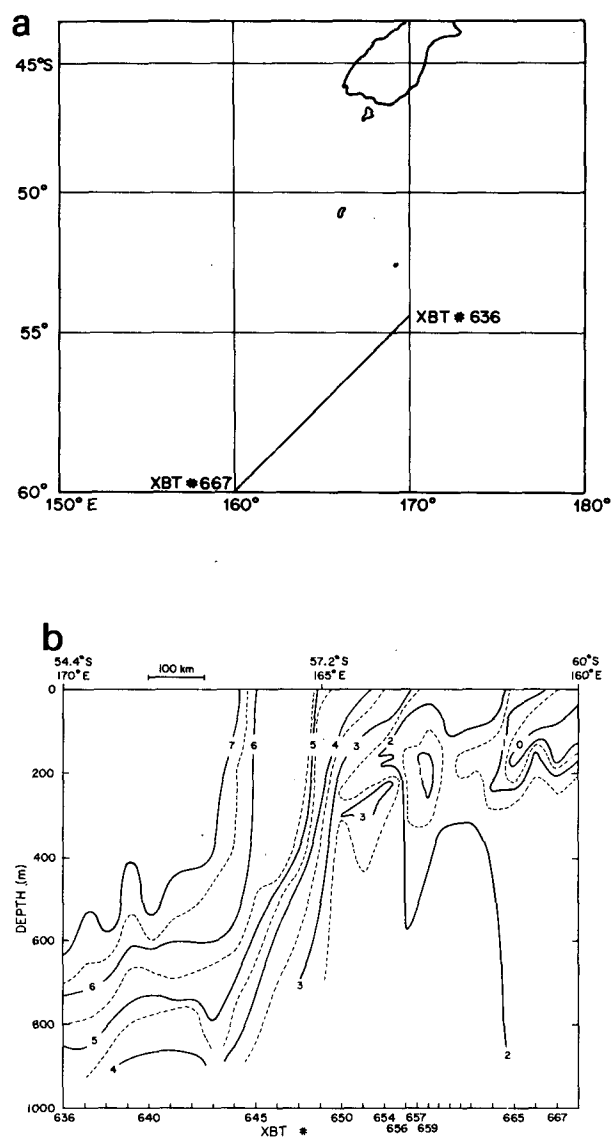

FIG. 2. The station position map (a), and temperature section (b), from a preliminary XBT survey of the frontal zones south of New Zealand. Measurements were taken in the front near XBT 650 in (b).

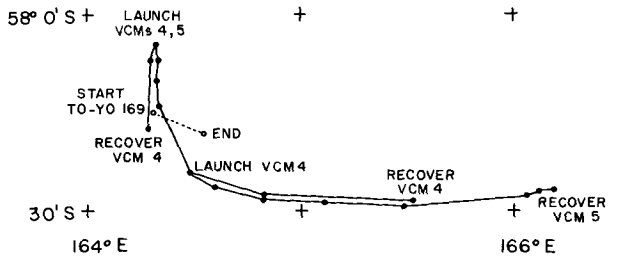

FIG. 3. Drift tracks of VCM's deployed in the frontal zone and CTD station positions south of New Zealand. Data from CTD To-Yo 169 are discussed here.

The structure of the Antarctic Polar Front south of New Zealand differs from that in the Drake Passage in that the termination of the temperature-minimum layer does not always coincide with the region of largest frontal gradients. (Burling, 1961). Large horizontal gradients may be associated with temperatures anywhere from 3 to 7°C (Heath, 1979). The frontal features in this region have been termed the primary and secondary polar front zones (Gordon, 1971) and the Australasian subantarctic front (Burling, 1961; McCartney, 1977).

A preliminary XBT section was run on the *Knorr* cruise to locate the front, Fig. 2. This section exhibits the complicated frontal structure described above. A small enhancement of lateral gradients is visible about the 6.5°C isotherm at the southern border of a large pool of nearly isothermal water. McCartney (1977) would term this pool the local version of Subantarctic Mode Water. The largest horizontal temperature gradient occurs between XBT's 647 and 650 about the 4°C isotherm. This lateral gradient is about twice that observed in the Drake Passage before the eddy formed. The buoyancy period in the frontal zone was 30 min, half that observed in the Drake Passage.

After an XBT survey and CTD section were completed, VCM's were deployed in the frontal zone at depths of 217, 400 and 630 m (Fig. 3). The floats were located on the cold side of the large horizontal gradient at 4°C seen in Fig. 2. The shallower float, VCM 5, was in the water for 4½ days while a second float was deployed twice. Vertical shear in the horizontal current necessitated the redeployment of the deeper float to minimize the horizontal distance between the two floats. The floats drifted south for a day and a half when first deployed, then turned abruptly and drifted for the remainder of the observation time nearly due east. The data discussed below were obtained prior to the turn of the VCM's.

3. Intrusion time scales

Several experiments were performed on the *Thompson* cruise to measure the decay time scale for the intrusions. Ideally, one would like measurements of an isolated fluid parcel with anomalous thermohaline properties in a quiescent homogeneous water mass. The data have none of these characteristics. First, the mean horizontal flow in the polar front is strong and has shear in the vertical (JZT). Superimposed on the mean flow are high-wavenumber high-frequency fluctuations due to internal waves. The effects of advection have been partially circumvented in this analysis since all measurements were made by, or relative to, neutrally buoyant floats deployed in the interleaving zone. Second, the intrusions sampled were located in the frontal zone which is capable of supporting growing intrusions (Toole and Georgi, 1981). Some of the data exhibit apparent intrusion growth, rather than decay, making interpretation of the data difficult.

A 16-cast CTD time series, with profiles taken about every two hours, was made in the Drake Passage after the formation of the cyclonic ring, while the ship maintained position relative to a VCM at 400 m depth. The potential temperature profiles from the series, processed to remove internal-wave vertical displacements as by JZT, appear in Fig. 4. In this process, the vertical coordinate of each cast is stretched so that its potential-density profile on vertical scales >100 m is identical to the ensemble-mean density profile of the casts in the series. This technique is described more fully in Toole (1980).

The intrusions observed in the re-established front seem to be of a much different character from that of those observed by JZT before the ring event. The profiles from their series are also shown in Fig. 4 for comparison. Individual intrusions have smaller thermohaline anomalies than in the first time series and appear to have smaller vertical scales. Temperature and salinity spectra of the data in the interleaving range (250–550 db) are red with a wavenumber slope between −2 and −3 (Fig. 5). The level of the spectra from this time series is significantly below that of the JZT series (Fig. 5) on scales greater than 60 m but the two sets of spectra are indistinguishable at the 95% confidence level on smaller scales. Temperature and salinity-gradient spectra showed a dominant wavelength of order 60 m which is significantly smaller than the 100 m wavelength scales found by JZT.

The common way to study temporal persistence is to compute the averaged dropped lagged coherence (e.g., Hayes, 1975). However, it is incorrect to use this method straightforwardly in this case because of spatial variability in the profiles. During each CTD station, one hydrophone was left in the water to measure range to the float. The float ranges that appear below each temperature profile in Fig. 4a vary from 0 to 1.1 km with a mean

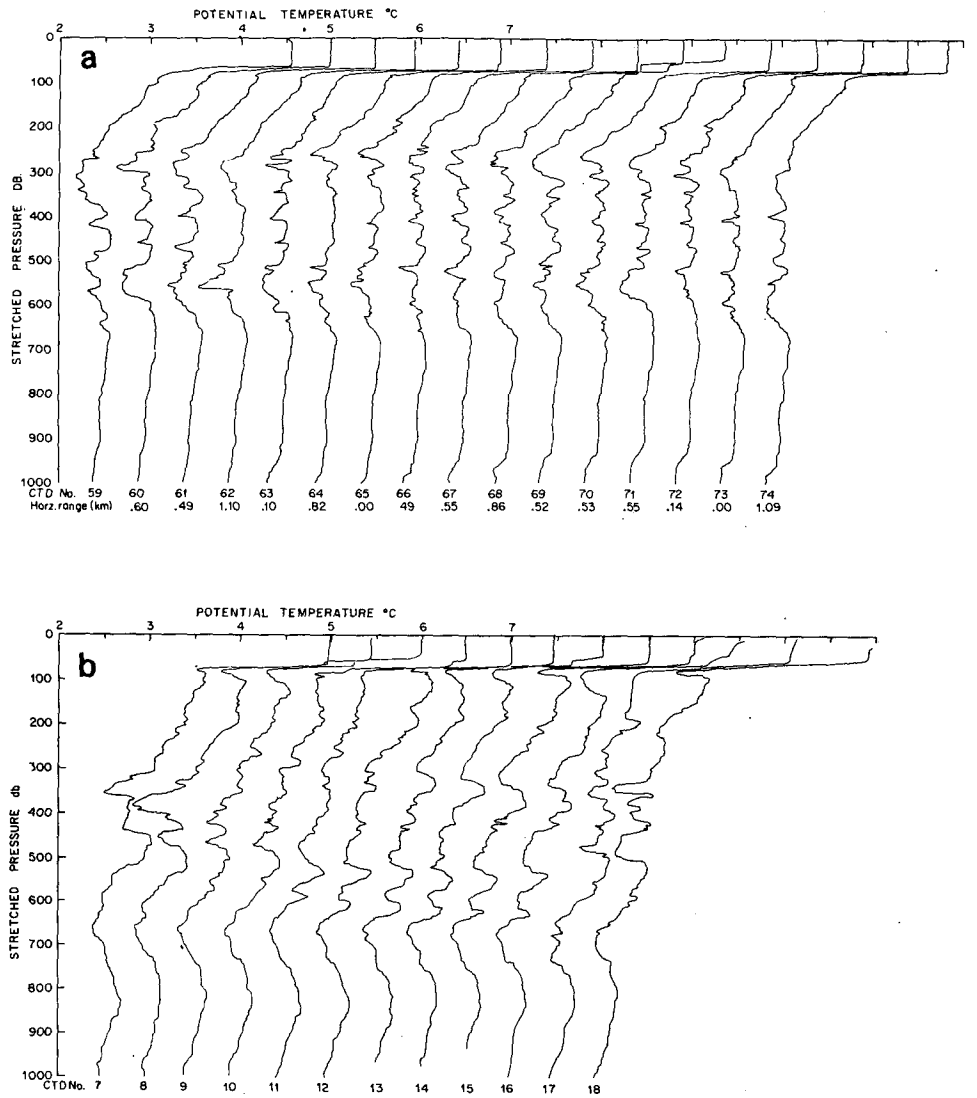

FIG. 4. Vertical profiles of potential temperature versus stretched pressure (see text) from the Drake Passage time series relative to a VCM at 400 db (a), and the profiles from the time series discussed by JZT (b). The temperature scales are correct for the first profiles and successive profiles have been offset by 0.5°C. The range between the ship and VCM at the time of the station is given below the profile in (a). VCM's were not deployed during JZT's time series.

of 0.52 km. Although small, these station ranges appear to be a significant fraction of the horizontal dimension of the intrusions during this phase. Observe the variation of the thermal structure between stations 63 and 65. The thermal structure is highly coherent over the 4.6 h separating these stations made directly over the float. Station 64 made just 800 m away from these stations but between them in time, shows virtually no coherent thermal structure around the float depth (400 m), a state quite unlike the results of the time series discussed by JZT where the estimated intrusion length scale was order 8 km.

Despite the apparent small lateral scale of these features, the profiles taken near the float consistently show a cold intrusion at the float depth, although its thermal anomaly and vertical scale do change between observations. It is not clear whether these changes are temporal or the result of spatial variations sampled during the series. Nevertheless, these results suggest that features can persist for periods longer than 1½ days (the duration of this series).

Three additional CTD time series spanning longer time periods but with poorer temporal resolution were made relative to VCM's during earlier deployments in the Drake Passage. The potential-temperature profiles from these series are plotted versus potential density in Fig. 6. The intrusions about

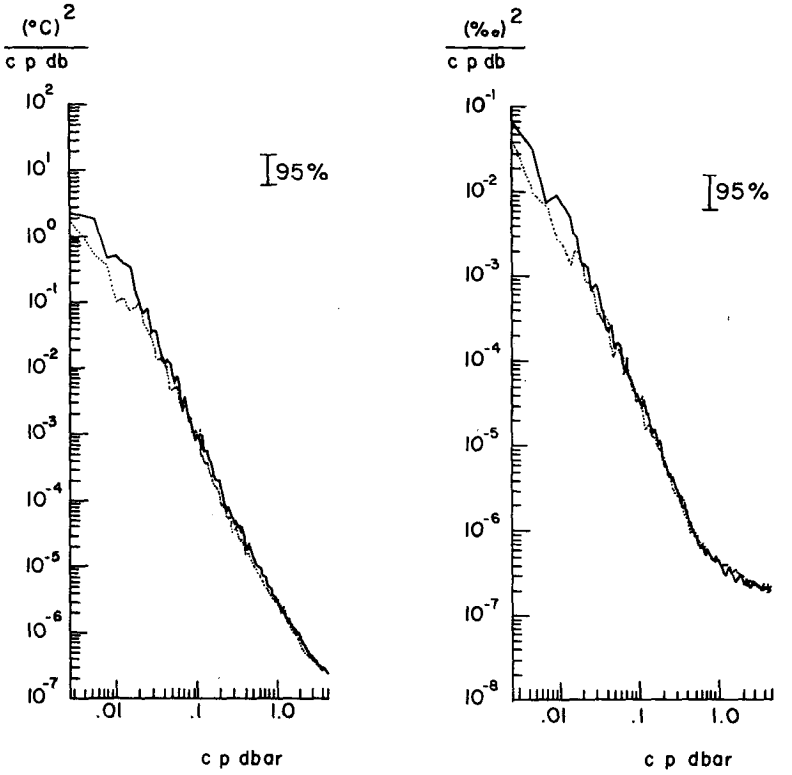

FIG. 5. Ensemble-averaged vertical spectra of temperature and salinity anomalies using data from the time series in JZT (solid line) and the time series discussed here (dotted line). Confidence bounds for the 95% significance levels are also given.

the depths of VCM 1 at station 44 are highly correlated with features at station 46 but bear little resemblance to those at station 52. Similarly for VCM 2, several features appear to persist from station 47 to station 51 but not throughout the float deployment. The intrusions about the depth of VCM 5 do not persist between casts. A cold feature below the float depth is visible at all three stations but the temperature anomaly of that feature increases during the time of observation.

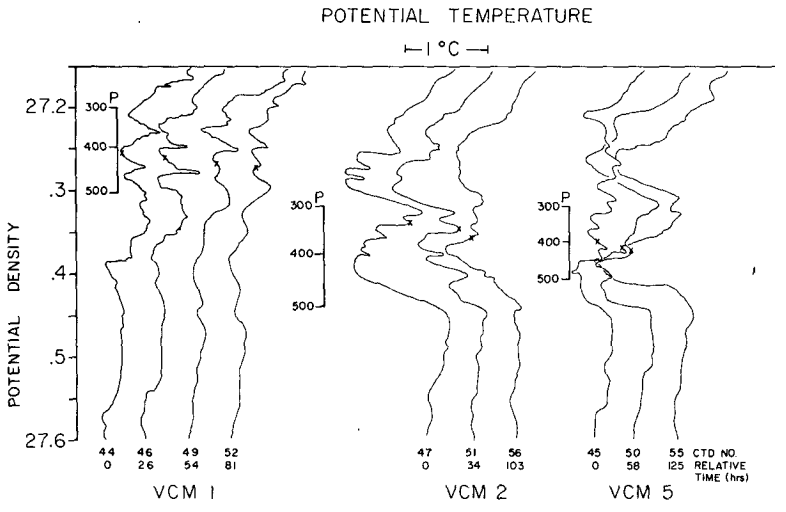

FIG. 6. Potential temperature profiles plotted versus potential density from stations made over VCM's. Also shown are approximate float depths (×) and pressure scales about the float depth. Successive profiles have been offset by 0.5°C and the relative timing of each station is given below the profile.

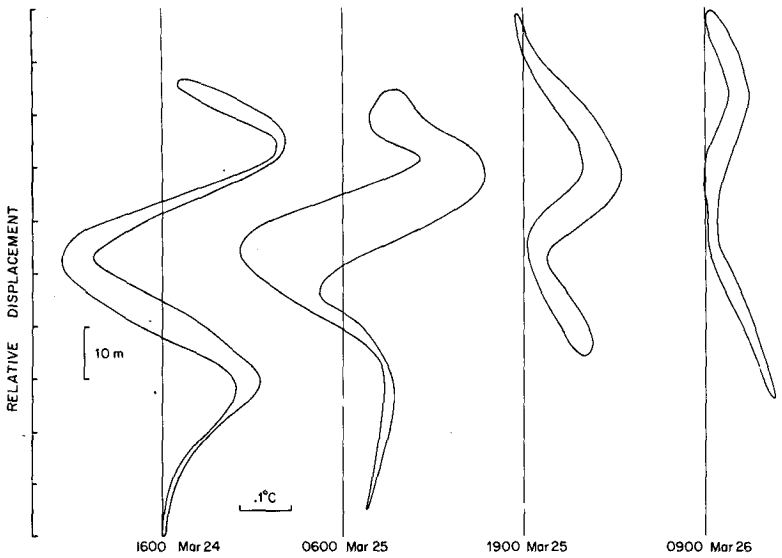

FIG. 7. Relative temperature data from a VCM plotted versus the relative vertical displacement between the float and the water in 12 h averages. The vertical lines through each profile demark the same temperature, while the mean times for the profiles are shown below. Only outlines containing some 90% of the data are shown because of time-response errors in the data.

The VCM's also yielded data on the time scale of the intrusions directly from their temperature records. Since VCM's tend to remain on isobars, the floats profile small regions of the water column around their mean depths as internal waves displace fluid past them (Voorhis, 1971). The VCM senses both temperature and relative vertical displacement so it is possible to produce plots of the vertical temperature profile about the float depth and to observe their change with time. This is difficult to do in practice, however, because of the long response time of the VCM thermistor (Toole, 1980).

The lag-corrected temperature data from the first deployment of VCM 1 is plotted versus relative displacement in 10–12 h averages in Fig. 7. Because of the lag correction problem, only the outline of the traces including some 90% of the data is shown in the figure. The reduction in the amplitude of the temperature signal found in the temperature profiles taken near this float (Fig. 6) is clearly seen in these data as a reduction in the amplitude of the thermal features around the float depth.

It is tempting to interpret this amplitude change as intrusion decay on a time scale of order two days but in this case also spatial variability could be responsible. Since VCM's do not follow fluid parcels through their vertical excursions, and generally sink slowly during their deployments, displacements between a fluid parcel and a VCM can be generated. Thus the persistence or decay time of order two days found here can be considered only a rough estimate. A truly Lagrangian float which follows fluid parcels vertically or an extensive dye experiment appears necessary to obtain more accurate results.

4. Spatial structure of intrusions

a. Drake Passage

It has been noted above that there was a great deal of spatial variation in the intrusion field during the 16-cast CTD time series. The horizontal length scale of the intrusions appeared to be of the same order as the ship-float ranges during the CTD casts. Careful examination of the profiles revealed station-to-station variations of the depths of the persistent features. The vertical coordinate in Fig. 4 is related to potential density, so depth variations in features imply density changes of the features. Since there is no steady trend to the depths of features with time, the data must be interpreted as a random sampling of features sloping in space rather than the observation of features propagating across density surfaces with time.

Following JZT, the slopes of these intrusions across the front relative to potential-density surfaces were computed by Toole, 1980. As in JZT, the intrusions were found to slope downward to the north. Recall, though, that the local horizontal temperature gradient had the opposite sign from that in JZT. This implies that cold intrusions in this region were sloping down toward cold water, seemingly in the wrong sense for driving by salt fingers.

b. South of New Zealand

The analysis of the Drake Passage data suggested that intrusions do slope relative to density surfaces but that the direction of that slope with respect to the large-scale density field could not be consistently

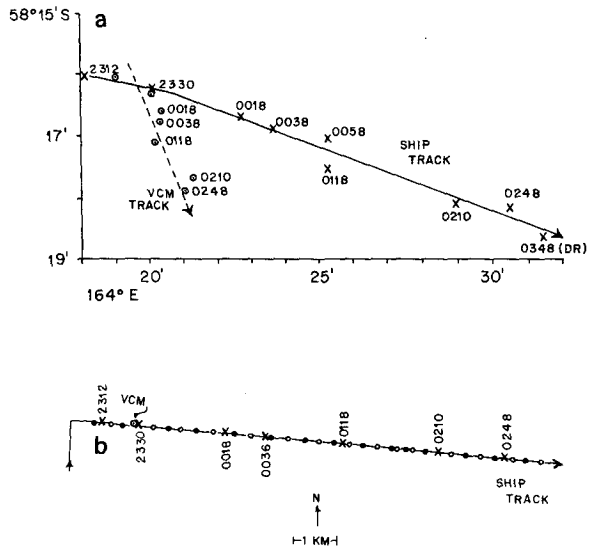

FIG. 8. The ship and float-drift tracks in absolute coordinates during the To-Yo experiment (a), and the ship track relative to the float (b). Satellite fixes for the ship with the times when they occurred are marked with crosses in (a) while dots mark the position of the VCM at the times of the satellite fixes inferred from float range and bearing data. Smooth lines have been drawn through the fixes to approximate the absolute ship and float tracks in (a). The range and bearing of the ship with respect to the VCM at the times of satellite fixes are denoted by the crosses in (b) while the ship's relative position when the CTD was at its shallowest and deepest depths are given by closed and open circles, respectively.

estimated. These slope estimates were also contaminated by temporal variations since the experiments used to estimate the slopes included data separated in time by many hours. Several small-scale CTD surveys were performed during the *Knorr* cruise to measure directly the intrusion length scales and their slopes across density surfaces on a time scale where intrusion decay could be neglected. These experiments involved cycling the CTD over a 500 db pressure range while towing the CTD across the front.

The towed Yo-Yo or To-Yo data discussed here (station 169 in Fig. 3) were taken one day after the VCM's had been deployed. Float tracks and XBT's were used to determine the orientation of the front prior to the tow. The ship was directed along course 090°, perpendicular to the front, heading toward warmer water. Figs 8a and 8b present ship and float tracks in absolute coordinates and in a frame fixed with respect to the VCM. Several satellite fixes (the only method of navigation in this area) arrived during the time of observation and these were used to plot the absolute position map, Fig. 8a. Because 1–2 km position errors are present in these data, a smooth curve is drawn through the various fixes to approximate the ship track. The VCM positions at the times of the satellite fixes, computed using ship-float range and bearing data are denoted by the ×'s in Fig. 8a. Some of the scatter in the float position is probably due to errors of ship's position. On the scale of the To-Yo, these position maps show that the ship course was within 15° of the cross-front direction. The map of the entire float track (Fig. 3), shows the To-Yo was made just north of a region where the current turned sharply to the east. This makes it less certain how the To-Yo was oriented with respect to the front on a larger scale.

The CTD To-Yo data were broken up into down- and up-traces, processed into a set of 29 traces with

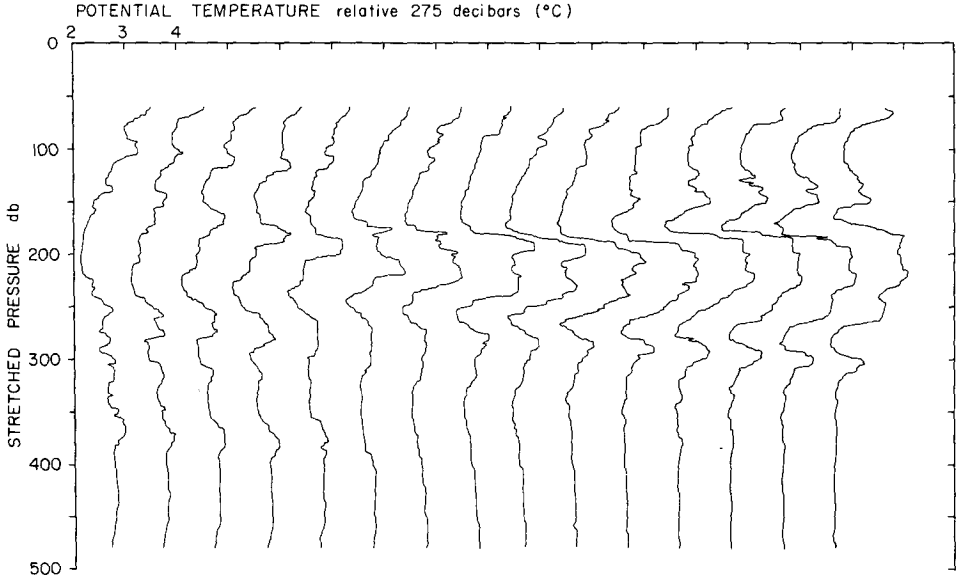

FIG. 9. Vertical profiles of potential temperature versus stretched pressure from the Yo-To experiment. Successive profiles have been offset by 1.0°C.

uniformly increasing pressure, and stretched to remove internal wave distortions. The potential temperature profiles for the down-traces shown in Fig. 9 extend for ~10 km across the front, with average profile separations of 0.75 km. Several features can be observed in the profiles extending a significant distance along the To-Yo track. In addition, the features are seen to slope in the vertical, which in these coordinates means they cross density surfaces. The duration of the To-Yo (5 h) was only a third of the local inertial period and small compared to an intrusion lifetime (see above), so these data may be viewed as a snapshot of intrusions sloping across density surfaces.

The average temperature gradient spectrum, computed from 409.6 db pieces (Fig. 10) has structure similar to the Drake Passage data. The spectrum shows enhanced energy density on scales between 200 and 30 m, comparable to the scales observed in the first time series in the Drake Passage discussed by JZT. The energy density for these data, though, is almost 10 times larger than that observed in the Drake Passage.

The dropped lagged coherence was computed to estimate the horizontal scales of the intrusions by averaging over 0.5 km bands of horizontal separation and four wavenumber bands [0.0024–0.0049, 0.0049–0.0098, 0.0098–0.0195, 0.0195–0.0391 (units: cpdb—cycles per decibar)]. The down- and up-traces are physically different since they slope through space in opposite directions. The coherences between down- and up-traces were only computed for the shortest space lag. Fig. 11 presents the coherence versus separation for the four wavenumber bands above. The average coherence between successive traces on scales <25 m was not significantly different from zero, in general. The coherence is seen to fall with increasing separation but the fall-off is not ordered in wavelength. The features of wavelength 100–50 m extend much farther across the section than the larger or smaller features.

Length scales for the intrusions were estimated with the separation for which the dropped lagged coherence was indistinguishable from zero at the 95% significance level assuming all station pairs were independent. The results are given in Table 1 for the four wavelength bands along with the resultant aspect ratios of the features. The intrusions are much longer than previously observed. Georgi (1978) estimated aspect ratios for XBT survey data with a horizontal length scale chosen

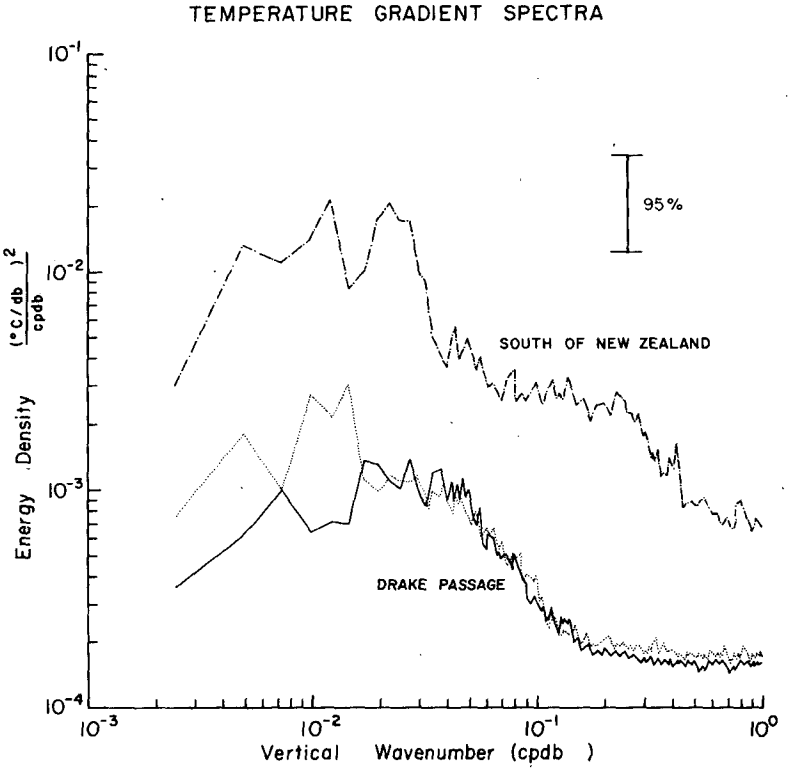

FIG. 10. Ensemble-averaged vertical-temperature-gradient spectra from south of New Zealand and from the two time series in the Drake Passage. The dotted line is from JZT's series while the solid line is from the series reported here. Also shown are the 95% confidence bounds for the spectra.

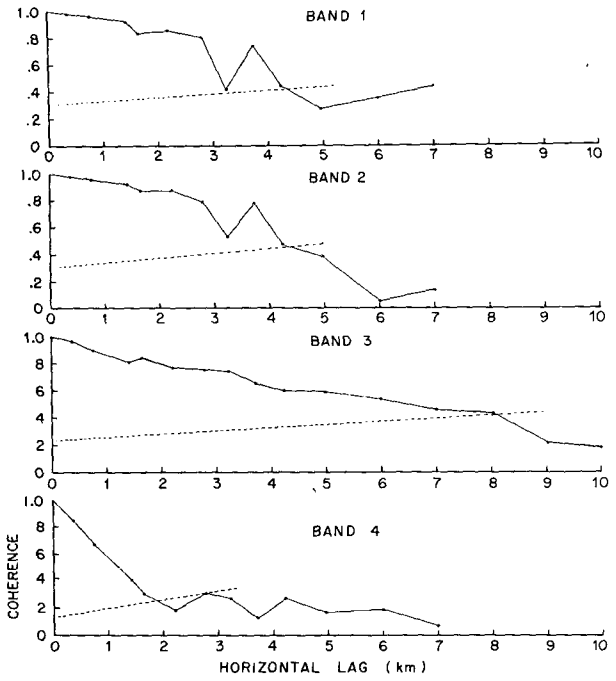

FIG. 11. Band-averaged coherence between station pairs versus horizontal separation using data from the To-Yo experiment. Band 1 includes wavelengths from 409.6–204.8 m; band 2: 204.8–102.4 m; band 3: 102.4–51.2 m; and band 4: 51.2–25.6 m. Data points above the dashed lines are significantly different from zero at the 95% significance level, assuming all station pairs are independent.

where the squared coherence equaled 0.5. Using this length scale, the aspect ratios of the present data are still smaller.

The intrusions pictured in Fig. 9 generally slope downwards from left to right. This is consistent with the idea that the intrusions are driven by salt fingering. The major exception to this observation is the cold feature appearing at the end of the To-Yo around 175 db. If we are to retain the idea of salt finger fluxes driving intrusions, then this feature must be thought of as an isolated cold leaf, advected along the front into the To-Yo path. This appears reasonable since this cold intrusion cannot be connected to the cold water across the front in Fig. 9. The other major intrusions can be connected across the front along the To-Yo path to their apparent sources.

The first 10 lowerings were not contaminated by this cold leaf so these data were used to estimate the cross-density slope of the intrusions. The dropped lagged coherence including all station pairs in this group was again calculated for the three wavenumber bands containing most of the temperature finestructure (bands 2, 3, and 4). Fig. 12 shows the phase angle plotted versus horizontal separation from this calculation along with least squares regression lines for each wavenumber band. The intrusion slopes determined from the regression lines are also presented in Table 1. Note that the intrusions with the smaller vertical scale slope most steeply across density surfaces. This can be observed in the profiles themselves in Fig. 9 where the small intrusion at 175 db in the fourth profile appears to slope more steeply than the larger intrusion at 230 db. The behavior of intrusions appears to depend on the vertical scale of the features.

TABLE 1. Estimates of intrusion length scales, aspect ratios and cross-isopycnal slopes from the To-Yo experiment.

Wavelength (m)	Length scale (km)	Aspect ratio	Intrusion slope
409.6–204.8	4.0	0.05	—
204.8–102.4	4.0	0.03	4.6×10^{-3}
102.4–51.2	8.0	0.01	6.7×10^{-3}
51.2–25.6	1.5	0.02	9.0×10^{-3}

5. Evidence for salt fingering

The vertical thermohaline gradients at intrusion interfaces are of the correct sense to support both types of double-diffusive phenomena (Stern, 1960; Turner and Stommel, 1964). There are several pieces of circumstantial evidence suggesting that at least salt fingering is active in the Antarctic Polar Front.

Linden (1974) has demonstrated that salt fingering (or salt sheeting) will be present in a region where temperature and salinity increase upwards even if a steady vertical shear is applied to the fluid. Only a continuous, highly turbulent velocity field appears able to disrupt the fingers in the laboratory (Linden, 1971), but the ocean is only rarely turbulent on small scales (see Gregg and Briscoe, 1979). In addition, Schmitt (1979a,b) has shown that the growth rate of the fingers is rapid with respect to the time scale of the oceanic shear and the fingers can effect significant mixing provided the stability ratio (the ratio of the vertical temperature and salinity gradients nondimensionalized by the thermal-expansion and saline-contraction coefficients) is below 2. Since intrusions are nearly density-compensating and the mean density stratification of the polar front is weak, salt finger fluxes in the intrusion field can be large.

The double-diffusive mechanisms flux heat and salt vertically at different rates. The laboratory measurements of salt fingering by Turner (1967) and Schmitt (1979b) yielded a lower bound on the ratio of nondimensional fluxes of heat (αF_T) and salt (βF_S) of $(\alpha F_T/\beta F_S) \approx 0.56$, where α and β are the thermal-expansion and saline-contraction coefficients. Turner (1965) also measured the vertical heat and salt fluxes through a diffusive interface

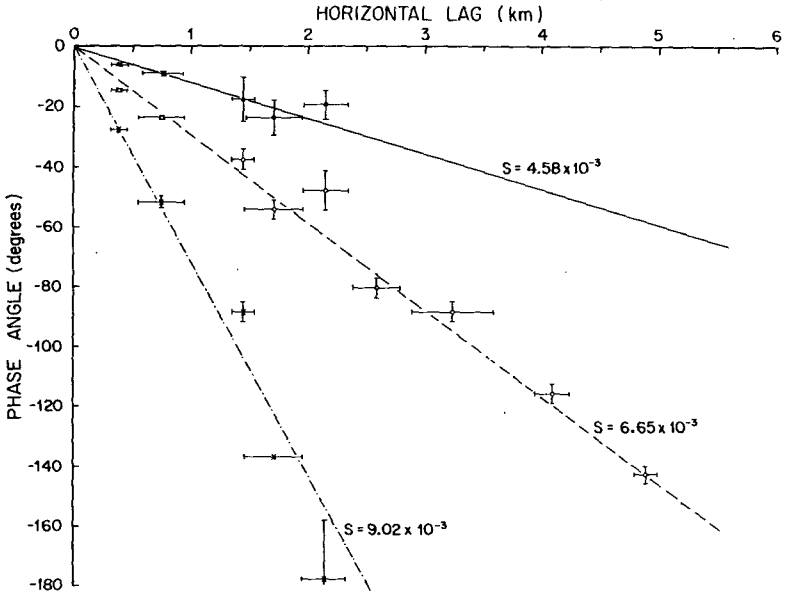

FIG. 12. Average phase angle between station pairs in the To-Yo experiment versus horizontal separation for wavenumber bands 2 (closed circles) 3 (open circles) and 4 (×). Error bars are shown for the 95% confidence bands. Intrusion slope estimates from the least-squares linear fits to the data are also given.

and found an upper bound on the flux ratio of 6.67. The change of an intrusion's temperature or salinity by vertical processes depends on the fluxes of temperature and salinity across the upper and lower interfaces of the intrusion. From the above experimental results, the flux ratio for an intrusion affected only by double-diffusive fluxes is bounded by

$$0.56 \leq \frac{\Delta\alpha F_T}{\Delta\beta F_S} \leq 6.67,$$

where the Δ indicates the difference in fluxes across the two interfaces. The laboratory studies of Turner (1978) show that, once formed, the total heat and salt fluxes into intrusions are dominated by transfers at the salt-fingering interfaces. Thus the flux ratio into the laboratory intrusions is only slightly larger than 0.56, and cold intrusions sink while warm intrusions rise. The sense of the intrusion slopes relative to density surfaces observed by JZT and in the data obtained south of New Zealand is consistent with Turner's laboratory results and the assumption that salt fingering is driving the intrusions.

Direct calculations of the heat and salt fluxes between intrusions using CTD data were not possible since the laboratory-derived formulas for these fluxes are in terms of the temperature and salinity jumps across an interface that are not easily identifiable or well resolved in CTD data. The flux ratio may be estimated if the intrusions are assumed to be locally steady. The nondimensional heat and salt conservation equations to lowest order are then

$$U\frac{\partial \alpha T}{\partial l} = \frac{\partial}{\partial Z}\alpha F_T,$$

$$U\frac{\partial \beta S}{\partial l} = \frac{\partial}{\partial Z}\beta F_S,$$

where U is the speed of intrusion advance and l is length directed along the intrusion while F_T and F_S represent the total vertical fluxes of heat and salt due to turbulence as well as double-diffusion. Vertically integrating over an intrusion, assuming U is constant, and dividing the two resulting expressions, yields

$$\frac{\frac{\partial}{\partial l}(\overline{\alpha T})}{\frac{\partial}{\partial l}(\overline{\beta S})} = \frac{\alpha(F_T^{SF} - F_T^D)}{\beta(F_S^{SF} - F_S^D)} = \frac{\Delta\alpha F_T}{\Delta\beta F_S},$$

where superscripts SF refer to the salt-fingering interface and D to the diffusive interface and the overbar is a vertical average. The flux ratio for an intrusion is then given in terms of the temperature and salinity gradients along the intrusion, provided entrainment does not drastically enlarge the thickness of the intrusion as it propagates. The studies of Ruddick and Turner (1979) show scale preservation once intrusions reach finite amplitude, suggesting the above relations are applicable.

The heat and salt content of four of the most persistent features in the To-Yo were computed from each profile by vertically averaging the temperature and salinity over a fixed vertical distance

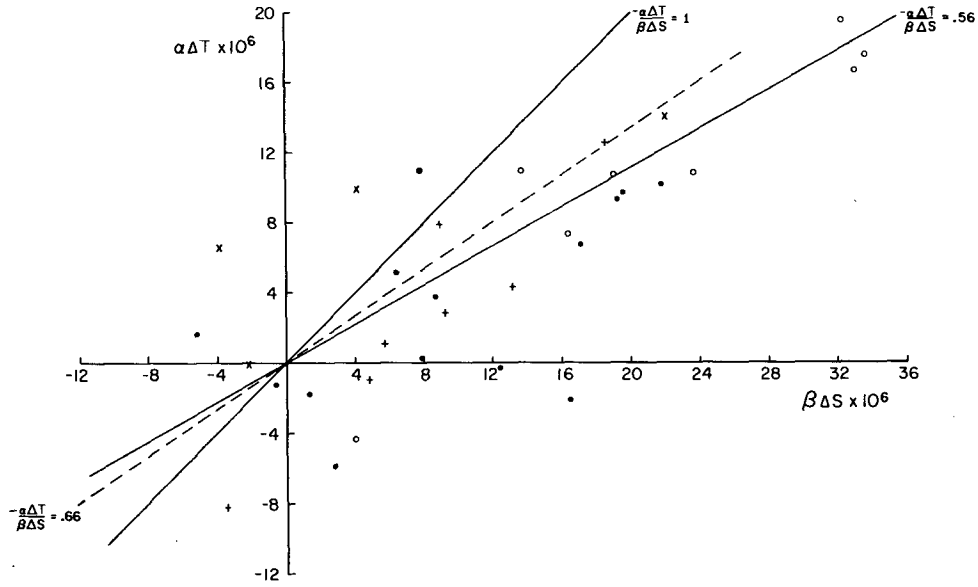

FIG. 13. A scatter diagram of nondimensional lateral temperatural difference to that for salinity along four selected intrusions observed in the To-Yo experiment. Reference lines are given for density-compensating temperature and salinity changes ($\alpha\Delta T/\beta\Delta S = 1.0$) and for the lower limit due to salt fingering ($\alpha\Delta T/\beta\Delta S = 0.56$). The line whose slope is given by the ratio of the variance in the two variables ($\alpha\Delta T/\beta\Delta S = 0.66$) is shown dashed.

centered at the temperature extremum of the feature. The temperature and salinity differences between adjacent observations of the same feature were computed and plotted on a scatter diagram (Fig. 13) after normalization by the local values of α and β. The data are noisy since there are large vertical gradients above and below the features. Small variations in the location of the averaging window could result in large differences of the calculated means. Nevertheless, the temperature- and salinity-difference data appear well correlated, especially for large differences where the noise errors are proportionally less. The flux ratio, estimated from the ratio of the standard deviations of the two data sets is 0.66 while the least-square slope estimates that bound this value are 0.84 and 0.53. A line with a slope of 0.66 is shown in Fig. 13 along with lines for the lower bound for salt fingering, a slope of 0.56, and for no density flux, a slope of 1.0. The flux ratio of 0.66 for these four intrusions appears consistent with double-diffusive mixing that is dominated by salt fingering.

6. Discussion and summary

Several experiments have been discussed in which the length scales of the finestructure and the slope of the intrusions across density surfaces have been estimated. The data of JZT and from the To-Yo exhibited dominant vertical scales of order 100 m, lateral scales of several kilometers and intrusion slopes consistent with the hypothesis that cold (warm) intrusions sink (rise) as they move across the front. Other data from the Drake Passage showed smaller vertical- and horizontal-scale finestructure which also crossed density surfaces but the slopes of those features could not be consistently related to the large-scale frontal gradients. The finestructure in the 16-cast time series differs from those observed in the other two experiments in that it appears to be detached leaves of fluid rather than intrusive extensions of fluid across the front. This distinction may resolve the discrepancy in the observed intrusion slopes.

We consider two initial states; the first, a smooth water-mass front with crossfront temperature and salinity gradients but no alongfront variations, and the second, an isolated leaf of fluid with a temperature and salinity anomaly. A perturbation on the smooth front will tend to grow on account of the salt-finger fluxes across the perturbation's vertical interfaces as discussed by Turner (1978). The initial growth will be directed across the front drawing on the potential energy stored in the cross frontal thermohaline gradients. There intrusions will be observed to slope across the front in the manner discussed by JZT. The leaf, on the other hand, has similar lateral thermohaline gradients on all sides. Double-diffusive fluxes acting across the leaf interfaces will produce a density change in the leaf and the resulting buoyancy force will drive the leaf up or

down depending on its thermohaline anomaly. Any lateral gradient of the density flux into the leaf would produce a slope of the leaf across density surfaces. Such gradients could be produced by local thermohaline anomalies in the leaf or its environment, anomalies with no dependence on the large-scale fields. Thus an isolated leaf of fluid might slope in any direction, while an intrusion from a smooth front initially slopes across the frontal gradient field.

It is suggested that the isolated leaves of fluid are old intrusions that have been sheared and advected from their generation site. Most likely, this site is the region of largest lateral thermohaline gradients in the front. Consequently, fine-structure observations near large frontal gradients will be dominated by intrusions such as observed by JZT and in the To-Yo experiment. Observations far from large gradients will show isolated leaves with smaller amplitudes and scales, as seen in the 16-cast time series discussed above.

It is noteworthy that the finestructure south of New Zealand had amplitudes of order three times those found in the Drake Passage while the New Zealand frontal gradients were a factor of two greater than in the passage. Despite the difficulty in estimating horizontal gradients, these results suggest that intrusion amplitudes may be proportional to frontal gradients.

Joyce's (1977) statistical model predicts a lateral effective diffusivity due to intrusions. This diffusivity scales directly with the vertical-gradient variance in the intrusive field and a vertical mixing coefficient, and inversely with the square of the lateral gradients across the front. If intrusion amplitudes are proportional to lateral gradient, as these results suggest, Joyce's model predicts a constant eddy diffusivity due to intrusions, provided the decay rate of intrusions is constant. Additional observations are needed to determine accurately the decay processes and decay rates of intrusions and leaves in order to verify this result.

The observations of JZT and those presented here suggest that salt fingering is active in intrusions. The models of Stern (1967) and Toole and Georgi (1980) describe intrusions' initial growth driven by vertical salt-finger fluxes. The vertical scale and variation of cross-front intrusion slope with vertical scale predicted by Toole and Georgi (1980) is in good agreement with the observations discussed here. Additional observations are required, however, to determine if salt fingers are indeed present in the intrusions and if their vertical heat, salt, and density fluxes are significant to the dynamics of the intrusions.

Acknowledgments. This work was facilitated by numerous helpful suggestions from T. Joyce, D. Georgi, R. Millard, E. Horne and R. Schmitt. The technical assistance of J. Dean and the expert typing by R. Whitney are warmly acknowledged. The work reported here was accomplished while the author held a graduate research assistantship at the Woods Hole Oceanographic Institution supported by the National Science Foundation Grant OCE 77-28355. This paper was prepared while the author held a National Research Council Research Associateship at the Pacific Marine Environmental Laboratory. Partial support was provided by the Office of the International Decade of Ocean Exploration of the National Science Foundation under agreement OCE 77-22868.

REFERENCES

Bryden, H. L., and T. M. Joyce, 1979: Studies of eddies and interleaving water masses east and south of New Zealand. *Antarct. J. U.S.*, **14**, 117–119.

Burling, R. W., 1961: Hydrology of circumpolar waters south of New Zealand. *N.Z. Dep. Sci. Ind. Res. Bull.*, **143**, No. 10, 9–61.

Georgi, D. T., 1978: Finestructure in the Antarctic polar front zone: Its characteristics and possible relationship to internal waves. *J. Geophys. Res.*, **83**, 4579–4588.

Gordon, A. L., 1971: Antarctic polar front zone. *Antarctic Oceanology I*, J. L. Reid, Ed., *Antarctic Research Series*, No. 15, Amer. Geophys. U., 205–221.

——, D. T. Georgi and H. W. Taylor, 1977: Antarctic polar front zone in the western Scotia Sea—Summer 1975. *J. Phys. Oceanogr.*, **7**, 309–328.

Gregg, M. C., and M. G. Briscoe, 1979: Internal waves, finestructure, microstructure, and mixing in the ocean. *Rev. Geophys. Space Phys.*, **17**, 1524–1548.

Hayes, S. P., 1975: Preliminary measurements of the time lagged coherence of vertical temperature profiles. *J. Geophys. Res.*, **80**, 307–311.

Heath, R. A., 1979: Oceanic fronts in the New Zealand subantarctic region. *Abstracts and Timetables for the Interdisciplinary Symposia*, XVIIth General Assembly of IUGG, Canberra, Australia, 165 pp.

Horne, E. P. W., and J. M. Toole, 1980: Sensor response mismatches and lag correction techniques for temperature-salinity profilers. *J. Phys. Oceanogr.*, **10**, 1122–1130.

Joyce, T. M., 1976: Observations of the polar front during FDRAKE, 1976: R/V *Thompson* leg 3. *Antarct. J. U.S.*, **11**, 157–158.

——, 1977: A note on the lateral mixing of water masses. *J. Phys. Oceanogr.*, **7**, 626–629.

——, and S. L. Patterson, 1977: Cyclonic ring formation at the polar front in the Drake Passage. *Nature*, **265**, 131–133.

——, W. Zenk, and J. M. Toole, 1978: The anatomy of the Antarctic polar front in the Drake Passage. *J. Geophys. Res.*, **83**, 6093–6113.

Linden, P. F., 1971: Salt fingers in the presence of grid-generated turbulence. *J. Fluid Mech.*, **49**, 611–624.

——, 1974: Salt fingers in a steady shear flow. *Geophys. Fluid Dyn.*, **6**, 1–27.

McCartney, M. S., 1977: Subantarctic mode water. *A Voyage of Discovery*, M. Angel, Ed., Pergamon Press, 103–119.

Millard, R. C., J. M. Toole and M. Swartz, 1980: A fast responding temperature measurements system for CTD applications. *Ocean Eng.*, **7**, 413–427.

Patterson, S. L., and H. A. Sievers, 1976: Contributions of the AGS Yelcho to FDRAKE 1976. *Antarct. J. U.S.*, **11**, 158–159.

Ruddick, B. R., and J. S. Turner, 1979: The vertical length scale of double-diffusive intrusions. *Deep-Sea Res.*, **26**, 903–913.

Schmitt, R. W., 1979a: The growth rate of super-critical salt fingers. *Deep-Sea Res.*, **26**, 23–40.

——, 1979b: Flux measurements on salt fingers at an interface. *J. Mar. Res.*, **37**, 419–436.

Stern, M. E., 1960: The 'salt-fountain' and thermohaline convection. *Tellus*, **12**, 172–175.

——, 1967: Lateral mixing of water masses. *Deep-Sea Res.*, **14**, 747–753.

Toole, J. M., 1980: Wintertime convection and frontal interleaving in the Southern Ocean. Sc.D. dissertation, MIT/WHOI Joint Program in Oceanography, 326 pp.

——, and D. T. Georgi, 1980: On the dynamics and effects of double-diffusively driven intrusions. *Prog. Oceanogr.*, **10** (in press).

Turner, J. S., 1965: The coupled turbulent transports of salt and heat across a sharp density interface. *Int. J. Heat Mass Transfer*, **8**, 759–767.

——, 1967: Salt fingers across a density interface. *Deep-Sea Res.*, **14**, 599–611.

——, 1978: Double-diffusive intrusions into a density gradient. *J. Geophys. Res.*, **83**, 2887–2901.

——, and H. Stommel, 1964: A new case of convection in the presence of combined vertical salinity and temperature gradients. *Proc. Nat. Acad. Sci.*, **52**, 48–53.

Voorhis, A. D., 1971: Response characteristics of the neutrally buoyant float. Woods Hole Oceanogr. Inst. Tech. Rep. No. WHOI-71-73, 56 pp.